# The Hector Instrument: optical design of the new higher-resolution spectrograph

Ross Zhelem, Robert Content, Will Saunders, Jon Lawrence, Jessica Zheng, et al.

Ross Zhelem, Robert Content, Will Saunders, Jon Lawrence, Jessica Zheng, Julia Bryant, Joss Bland-Hawthorn, David Robertson, Mahesh Mohanan, Sudharshan Venkatesan, "The Hector Instrument: optical design of the new higher-resolution spectrograph," Proc. SPIE 11447, Ground-based and Airborne Instrumentation for Astronomy VIII, 114478U (13 December 2020); doi: 10.1117/12.2562634

SPIE.

Event: SPIE Astronomical Telescopes + Instrumentation, 2020, Online Only

# The Hector Instrument: optical design of the new higher-resolution spectrograph

Ross Zhelem*[a], Robert Content[a], Will Saunders[a], Jon Lawrence[a], Jessica Zheng[a], Julia Bryant[b], Joss Bland-Hawthorn[b], David Robertson[a], Mahesh Mohanan[a], Sudharshan Venkatesan[a]
[a]Australian Astronomical Optics, Macquarie University, 105 Delhi Rd, North Ryde, NSW 2113, Australia; [b]Sydney Institute for Astronomy, School of Physics, A28, The University of Sydney, NSW 2006, Australia

## ABSTRACT

The Hector instrument is the new multi-object facility at the Anglo-Australian Telescope. It consists of new-format hexabundle IFU's, complex robotic positioner with magnetic system, unique sky-fibre system, guiding system, optical cable and two spectrographs. Light is captured at the telescope prime focus by optical fiber imaging bundles (hexabundles) at f/3.25 and delivered to the spectrograph slit via ~50 m long fiber cable. At the spectrograph end, the fibers are reformatted into a curved slit relaying unconverted telescope input. The spectrograph optics includes fast collimators and cameras reimaging the slit onto 4k x 4k E2V detectors at f/1.3 with magnification 1/2.5. The challenge of good image quality with the large pupil size (180 mm) and the field of view (±12° at detector) was met by introduction of several aspheric surfaces in the all-refractive design. The blue and red arms, 372-591 nm and 571-778 nm, respectively, are implemented with the help of a dichroic beam splitter in the diverging beam followed by a collimating doublet lens for each arm. An upgrade is possible to the infra-red arm with the help of an additional dichroic beam splitter. The dispersers are asymmetric VPH gratings with slanted fringes optimised for the passband of each arm. Optical performance of the dichroic beamsplitter and gratings has been confirmed and complemented by in-house metrology. The spectrograph throughput is predicted based on transmittance of materials and coatings.

**Keywords:** spectrograph, IFU, multi-object, fiber slit, dichroic beamsplitter, VPH grating

## 1. INTRODUCTION

Hector will conduct an integral field spectroscopic survey of 15,000 galaxies of the Southern sky following up on the SAMI Galaxy Survey. The project scale and details have been refined and finalized[1-4]. The existing 2df facility will provide a wide field for the Hector survey. According to science requirements[1] most of the galaxies will be spatially resolved and will benefit from stellar and gas velocity maps. The telescope provides input suitable for direct injection into a fiber IFU. Hexabundles are hexagonally arranged fiber arrays that have been used and improved in capacity of IFUs for over a decade[4-5]. The IFU end of the fiber cable will be reconfigured by a positioner in the telescope focal plane. The fiber cable provides a flexible link between the telescope and the spectrograph.

The fiber feed allows the spectrograph to be stabilized and eliminate thermal variations and gravitational flexures. The spectrograph is assembled in a dedicated environmentally controlled location. The Hector instrument has two spectrographs, the existing AAOmega spectrograph, and a new higher-resolution fixed-format Hector spectrograph. The new Hector spectrograph is designed as a 2-arm (with an upgrade path to 3 arm) all-refractive instrument that delivers medium spectral resolution over the wavelength range 372 – 778 nm (992 nm with 3 arms). The spectrograph is fed by a custom optical cable with the slit made of 855 fibers for high-multiplex spectroscopy. In this paper we describe the design of the new spectrograph, trade-offs and stages of development and present the final optical design and performance that conforms to science requirements. Engineering aspects of the spectrograph optics are also discussed. All optical elements for the spectrograph have been received, and the flat optics have been characterized by means of full aperture interferometry and photometry. Spectrograph current status and brief assembly, integration and testing plan are presented here.

*ross.zhelem@mq.edu.au; phone 61 2 9372 4872; aao.org.au/macquarie

Ground-based and Airborne Instrumentation for Astronomy VIII, edited by Christopher J. Evans, Julia J. Bryant, Kentaro Motohara, Proc. of SPIE Vol. 11447, 114478U · © 2020 SPIE · CCC code: 0277-786X/20/$21 · doi: 10.1117/12.2562634

## 2. HECTOR SPECTROGRAPH OPTICAL DESIGN

The Hector spectrograph is a 2 arm design with a fiber input slit and an upgrade path to a 3 arm design. The fiber core is reimaged by the spectrograph optics onto the CCD detector, while the fiber far field forms the pupil which is projected by the spectrograph collimator onto the VPH gratings, dispersing the beam into the cameras. The design operates with two semi-custom Spectral Instrument Dewar detectors. The red and blue spectrograph cameras provide demagnification of the fibre slit and are therefore a more challenging design when compared to the collimator. Each camera images the spectra on a 4k x 4k E2V detector. The average resolution is 0.13 nm. The wavelength range is from 372 nm to 778 nm with the dichroic crossover at 581 nm and a common region to both cameras from 571 nm to 591 nm; implementation of the 3rd arm would extend the wavelength coverage to 992 nm. The cut-off wavelength was chosen based on science requirements and to minimize the overlapping region. This in turn maximizes the resolution of the spectrograph for the same spectral length in each pixel. In order to produce quality spectra with a reduced number of optical elements, the Hector spectrograph relies upon aspheric surfaces in both the collimator and camera. The fibre core size is 103 µm which corresponds to 1.6" on the sky.

The spectrograph optical design is the outcome of scrupulous three stage development with analysis of trade-offs, performance drivers, and cost minimization[6-7]. Initially, it was considered to use a microlens array slit which would allow to reduce the numerical aperture of the fiber output and simplify the design of the collimator. Microlens arrays are precision optics lithographically etched to custom requirements, the savings on collimator fabrication would be offset by the relatively high cost of the microlens array. Tolerances of a system with microlens arrays on input and output also degrade the performances. For example, manufacturers guarantee variation of radius of curvature across only to within 5% with a practically achievable value of 2.5%. Preference was given to a fast collimator with direct fiber output.

Several layouts of the spectrograph produced during the design phase, were modifications of two major approaches, namely, transparent and semi-transparent. The latter included a reflective collimator used off-axis and consequently, the collimator required an off-axis Schmidt corrector. In the semi-transparent design, VPH gratings were supposed to be bonded to a prism making a grism, this was less desirable from a risk mitigation standpoint. All surfaces were aspheric and the design contained large doublets to be bonded or greased. Cost evaluation also showed that the semi-transparent design was more expensive than the transparent design.

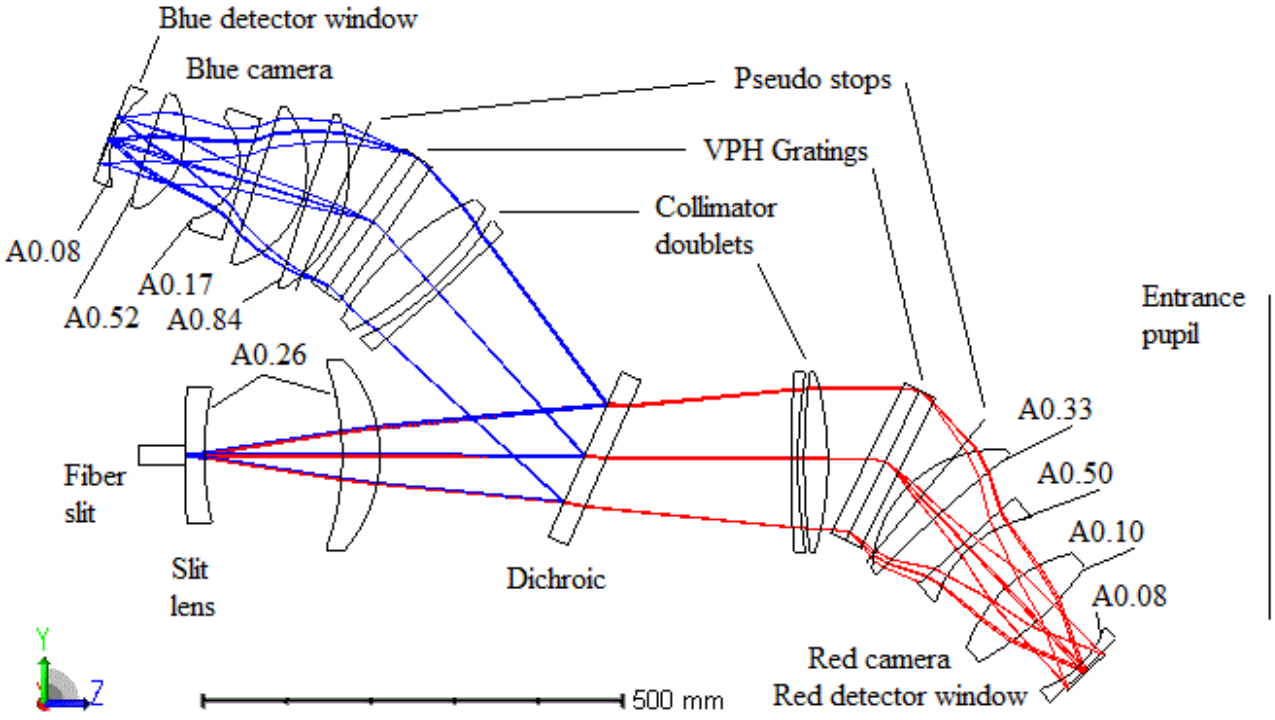


Figure 1. Hector spectrograph optical layout. View from above. "A" stands for an aspheric surface with the maximum departure from best fit sphere in mm.

The transparent design consisted of singlet lenses only in the collimator and cameras. The design featured just 6 mild aspheric surfaces for efficient fabrication. There was no clear pupil stop as compared to the semi-transparent design but this was overcome with the help of a pseudo-stop made of several baffles working together to truncate the peripheral areas of beams. The transparent version was selected for further development in the last stage to yield a hybrid design for the spectrograph. The hybrid design borrowed a number of features from the semi-transparent design. The aspheric departure was increased in pursuit of image quality and lower cost because it permits to reduce the size of the optics for the same performances. The detector windows became thin in the center and the detector was pushed close to the window to reduce separation. Additionally, the dichroic beamsplitter was moved from the collimated space in front of a VPH grating and inserted into the diverging beam before the collimator doublet. In so doing, blue and red spectrograph arms now require individual collimating air-spaced doublets but the overall cost remained about the same, even became slightly smaller. The benefits in performances of this configuration are the reduction of the range of incidence angles improving performance in the transitional crossover area, and the smaller wavelength range of the doublets. The final design is displayed in Figure 1.

### 2.1 Fiber slit

The spectrograph is located in a dedicated environmentally controlled room and it is linked to the telescope via flexible optical fiber feed. On the spectrograph end, all the fibers are terminated into a slit according to the configuration shown in Figure 2 in projection on the adjacent surface of the slit lens (Figure 1). Fiber cores follow the curved path with the total length of 145.2 mm and 3.3 mm sag of the middle with respect to the edges. The curvature is implemented by a number of identical slitlets each one housing a linear array of fibers. The fibers are placed tangentially to the design footprint so that the departures of fibers from their nominal positions are minimized.

Additionally, the front face of each slitlet is brought into tangential contact with the spherical surface of the slit lens pointing along the radius of curvature of that surface (Figure 1). This arrangement ensured that the entrance pupil for the spectrograph is coincident with the center of curvature. Slitlets are polished flat and point contact butting up against a spherical surface implies that peripheral fibers in each slitlet will be slightly out-of-focus in comparison with the central area where the contact takes place. The size of a slitlet was chosen to keep defocus as well as non-circularity of the fiber footprint within tolerable limits. The Hector spectrograph slit is designed to be an assembly of 19 V-grooved slitlets.

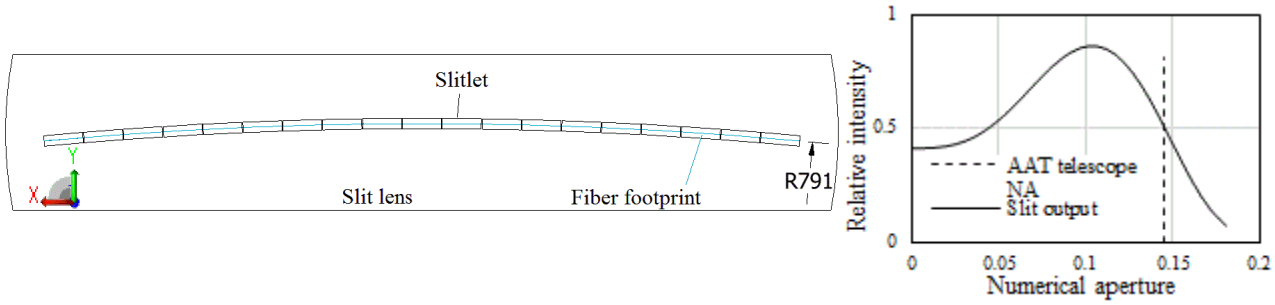


Figure 2. Layout of the curved fiber slit (left panel). Model of radial profile of telescope input at it emerges from the slit (right panel)

Commonly, a flat pupil illumination is assumed for optical designs resulting in possible variation of optical properties. Usually, the telescope direct feed is reasonably well represented by a flat far field. With a fiber cable relaying telescope input to the spectrograph, we expect pupil intensity variations introduced by the effect of focal ratio degradation due to inherent modal nature of light propagation in fibers. The focal ratio degradation of the fiber output depends significantly on both fiber brand and cable fabrication techniques. An average far field profile (Figure 2, right panel) has been determined experimentally from prior art. The focal ratio degradation redistributes the pupil illumination forming a ring and increasing the beam size as compared to the original telescope beam. These expected pupil intensity measurements are explicitly included in the design of the spectrograph.

### 2.2 Pseudo-stops

Pupil stops are important features of an optical system limiting the beam to the design dimensions. This is particularly important for a fiber fed instrument as the focal ratio degradation tends to increase the size of the beam. Light from the edges of an enlarged pupil is not accounted for in an optical design and therefore will cause image blur and loss of contrast.

The Hector spectrograph has a compact design with tight spacing between components. Consequently, a single pupil stop cannot be placed on or in front of gratings. The semi-transparent version discussed in Section 2, is based on the Schmidt camera principle and it features convenient, significant pupil relief. Separation of collimators and VPH gratings in the selected transparent design would create enough space for the stop but it would also increase the dimensions of optics and introduce extra constraints to achieve good imaging performance. A different approach is used here.

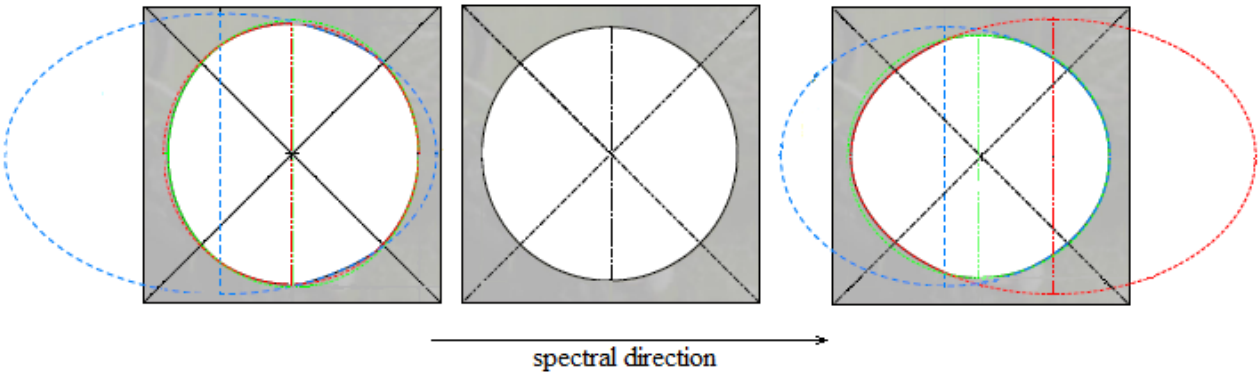


Figure 3. Stop apertures for the blue arm. Left: VPH grating, front surface. Middle: VPH grating, back surface. Right: camera pseudo-stop.

The optical conjugate of the entrance pupil is located after the VPH gratings in close proximity to the first lens of the cameras in both blue and red arms (Figure 1). Pseudo-stop apertures are placed in those locations. However, they cannot function as full stops due to the dispersion by the gratings. These pseudo-stops perform efficiently only in the spatial direction and are enlarged in the spectral direction to avoid significant vignetting. Another pseudo-stop is placed on the front side of each grating where it performs efficiently in the spectral direction and is enlarged in the spatial direction because the pupil is very much out of its focus at that position. At first, the design was made with a stop just after the fibers and no pseudo-stops. It had a larger NA than the input beam in the fibers from the telescope to capture some of the light dispersed by the focal ratio degradation but it also blocked some to limit the spectrograph NA. There is however a degradation of the image quality when this false stop is removed from the design and pseudo-stops that do not vignette any light are added. The pseudo-stops were then given more complex shapes that vignette more light and baffles also blocking more light were added after the gratings to bring back the original image quality. The shapes were carefully chosen (Figure 3) to minimize the losses of light resulting in an average transmission almost equal to that of the design with the false stop. Each aperture is the combination of several geometric shapes.

### 2.3 Image quality and spectral resolution

The spectrograph collimator and camera optics were optimized to produce excellent maximum and average image quality on 4K X 4K CCD detectors (Figure 4). The spot size is reasonably uniform across the entire field of view with the average RMS radius of 7.8 µm and 7.6 µm for blue and red cameras, respectively. Particular attention was given to spot symmetry and equalizing RMS values in x and y directions simultaneously using local and Hammer optimization techniques in Zemax optical design software. The design also reduces the elongation of PSFs at 45 degree which causes systematic errors when there is cross-contamination between spectra.

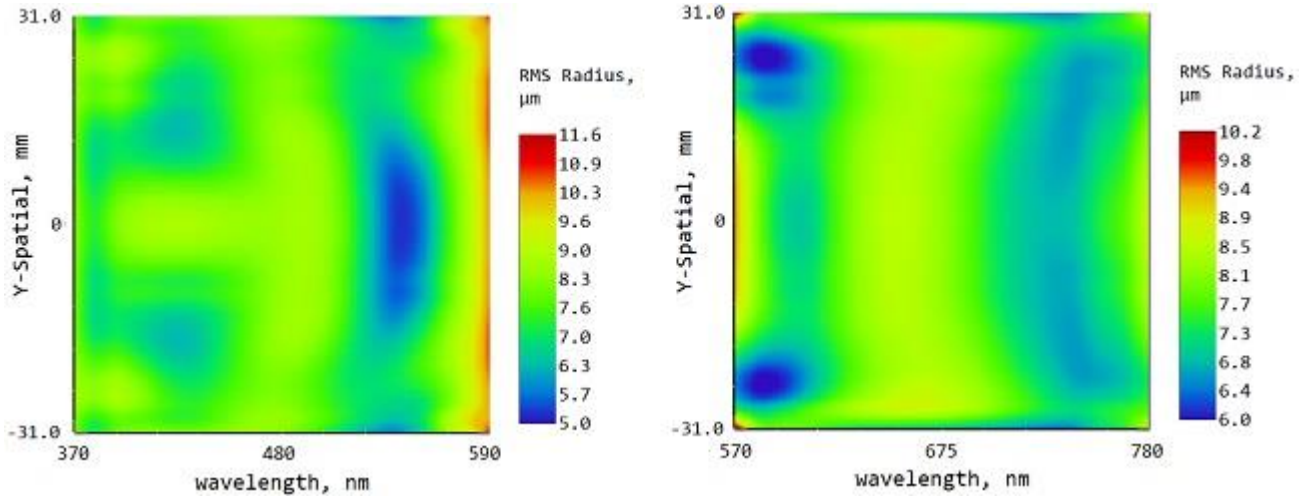


Figure 4. Image quality. Point Spread Function surface maps. Left: blue CCD. Right: red CCD. Note that the cutoff wavelength of the dichroic is at 581 nm so the regions of largest RMS are where the dichroic transmission is low.

Spectral resolution is determined by the resolution element which is the imaged size of the fiber core convolved with the point spread function of optical aberrations. The spectral resolution for the Hector project is defined as:

$$R = \frac{\lambda}{\frac{\sqrt{3}}{2}\Delta\lambda_{FWHM}}, \quad (1)$$

where: $\Delta\lambda_{FWHM}$ is the spectral width of the resolution element at FWHM measured from a radial profile,

$\sqrt{3}/2$ is the factor linking design and digital calculations.

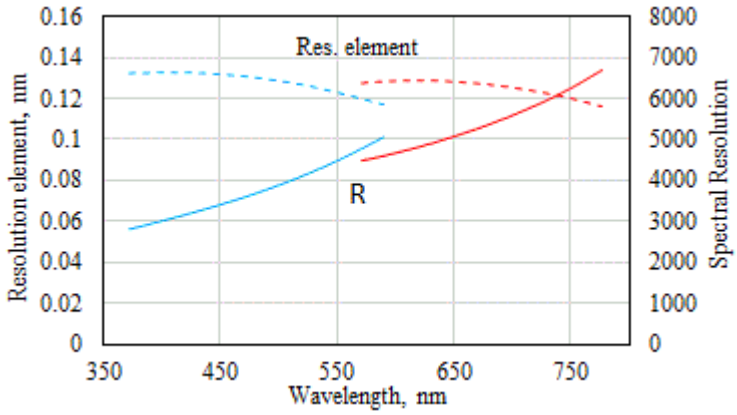


Figure 5. Hector spectrograph resolution parameters vs wavelength.

The link factor in Equation 1 is introduced for transition from the design definition to CCD image analysis. The following procedure is applied to a digital frame: a 2D resolution element is collapsed by summing pixels in spatial direction and the obtained 1D profile is analyzed to determine FWHM. The 2D to 1D conversion effectively reduces the profile width which effect is captured by the link factor. It should be noted that the factor is derived assuming that the image of a resolution element is a uniform circle. We accept this for the definition according to Equation 1.

The resolution element of the Hector spectra is nearly constant for all wavelengths (Figure 5) whereas the spectral resolution exhibits expected scaling proportionally to the wavelength.

### 2.4 Baseline optical specifications and science requirements

The design of the Hector spectrograph was driven by high level science requirements[1]. Table 1 lists related characteristics of the spectrograph as well as other optically significant parameters. The requested wavelength coverage, and the instrumental spectral resolution have been achieved.

Table 1. Summary of optical properties of the Hector spectrograph.

| | | |
|---|---|---|
| Field of view/Slit length | 145.2 mm | |
| Fiber core/cladding/buffer diameter | 103/123/250 µm | |
| Number of fibers | 855 | |
| Number of slitlets | 19 | |
| Fibers per slitlet | 45 | |
| Entrance Pupil Diameter | 390 mm | |
| Entrance Pupil Position: | 1270 mm | |
| Spectral arms | BLUE | RED |
| Wavelength range | 372 - 591 nm | 571 - 778 nm |
| Overlap between arms | 571 - 591 nm | |
| Dichroic split | 581 nm | |
| Collimator effective focal length | 592 mm | 560 mm |
| Camera effective focal length | 235 mm | 223 mm |
| Collimator F/# | 3.3 | |
| Camera F/# | 1.3 | |
| Slit magnification | 1/2.5 | |
| Collimated pupil diameter | 180 | 169 |
| Dichroic angle of incidence | 24 | |
| VPH grating line frequency | 1099.3 l/mm | 1178.5 l/mm |
| VPH angle of incidence | 13.5° | 26.3° |
| CCD to Detector window: | | |
| separation | 1.4 mm | 4 mm |
| decenter in spectral direction | 8.8 mm | 0.45 mm |
| CCD to camera: | | |
| tilt in spectral direction | 3.0° | 2.1° |
| CCD: | | |
| pixel size | 0.015 mm | |
| number of pixels | 4096 x 4096 | |
| linear dimensions | 61.4 x 61.4 mm | |

The optical design does not preclude a future upgrade path to extend the wavelength coverage to almost 1000 nm. The addition of the third infrared arm covering the wavelength range 758 – 1000 nm is enabled in the two arm version (Figure 1). An additional dichroic beamsplitter will be placed between the current dichroic and the red collimator doublet reflecting the red arm bandwidth at right angle. The existing red arm will be relocated to work in reflection from the new beamsplitter. The new infrared arm consisting of a collimator doublet, VPH grating, camera and detector, will replace the red arm in its current location.

## 3. SPECTROGRAPH OPTICS MANUFACTURING AND TESTING

The complete set of lens optics for the Hector spectrograph has been manufactured and delivered by Optimax Systems. There are 10 aspheric surfaces with aspheric departures up to 0.84 mm from best fit sphere. Full aperture metrology is critical for lens quality. The company provided the maps of each surface using industry standard aperture stitching

interferometer. The technique allows testing of any part without additional test optics, as is the case with null interferometry.

The lenses were specified to have at least 2 nm RMS surface micro-roughness which is the level of conventional pitch polishing. Reduced micro roughness is required to minimize the scattered light in the system. The delivered lenses of Hector spectrograph exceeded the requirement. The residual micro-roughness depends on lens material, polishing tools and compounds rather than surface figure. The micro-roughness of all lenses is in the range of 0.3 to 1.7 nm RMS.

Radii of curvature were specified at precision level (0.1%) and successfully met by the manufacturer. The remaining error may be compensated by respacing of lenses during as-built re-optimization. This option is not available for irregularities which remain uncorrected. Irregularity error is defined after focus subtraction and it must be small in comparison with the image quality requirements. Irregularity of the spheres is within 0.03 – 0.4 waves PV and that of aspheres is 0.06 – 0.85 waves PV. The design image quality of the Hector spectrograph ranges from 5 and 4 waves PV normalized to 633 nm and averaged over all wavelengths, for the blue and red arms, respectively. The spectrograph lenses are expected to have negligible effect on the image quality.

The efficient antireflective (AR) coatings are required to improve instrument throughput. They are specified for most of optics on a reduced bandwidth of the blue or red arm. Only two collimator lenses with the total of three surfaces operate across the full range with maximum reflectance 1.8%. The variety of substrate materials and angles of incidence called for 29 different coating designs for the spectrograph lenses. The blue or red AR coatings feature very low maximum reflectance within 0.35% - 0.6%. The camera lenses and detector windows are optically fast with angles of incidence ranging from normal up to 50 degrees. The vendor applied the coating taking into account the steep curvature toward the edges and the dimensions of the camera optics.

### 3.1 Full aperture interferometry and photometry

The Hector spectrograph optics are designed to work with the collimated pupil 180 mm in diameter to deliver required spectral resolution. The dichroic beam splitter is 220 mm in diameter. Although placed in a divergent path with smaller individual footprint, the large slit length increases the dimensions of the beamsplitter. The VPH gratings are 220 mm square.

A standard test and verification report from a vendor includes interferometry with 4 inch sub-apertures and photometric measurements of several zones ~1 inch in diameter. Sub-aperture interferometry is useful only if stitching capability is available to build a full aperture wavefront map. Likewise, zonal photometry covers a very small area of entire part for adequate statistical averaging. Given the size of the Hector beamsplitter and gratings we extended our in-house metrology of flat optics to the collimated beam of 200 mm in diameter.

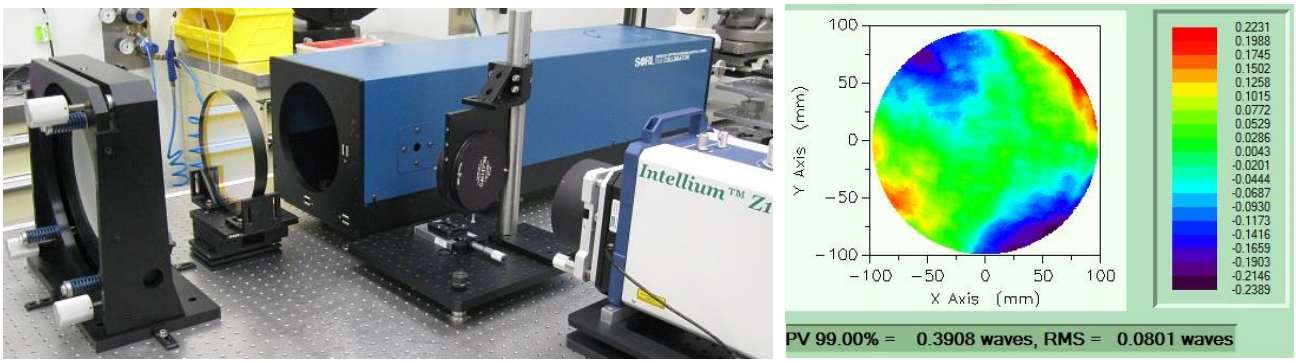


Figure 6. Full aperture interferometric setup for Hector beam splitter and VPH grating (left panel). Reference wavefront map, single pass (right panel)

The full aperture interferometric setup (Figure 6) consists of Intellium Z100 interferometer with 4 inch F/3.3 transmission sphere feeding an 8 inch off-axis parabola as the beam expander after reflection from a fold mirror. The test optics is placed in the collimated output followed by the return flat. The setup accumulates 0.39 wave PV error which is subtracted from optical path difference map to obtain the wavefront of a part under test.

Measurements of full aperture throughput require capability to capture a transmitted beam after the test optics. A light collector has been designed for this purpose. The principle of operation is shown in Figure 7 for the example of a VPH grating. The test beam from the off-axis collimator (Figure 6) is launched at a grating, beamsplitter or any flat optics. The output is collected by the condenser lenses placed in close proximity to the test optics. The condenser elements are off-the-shelf singlets assembled into a fast collecting lens with short effective focal length and back focus distance to minimize the length of spectrum dispersed by the grating.

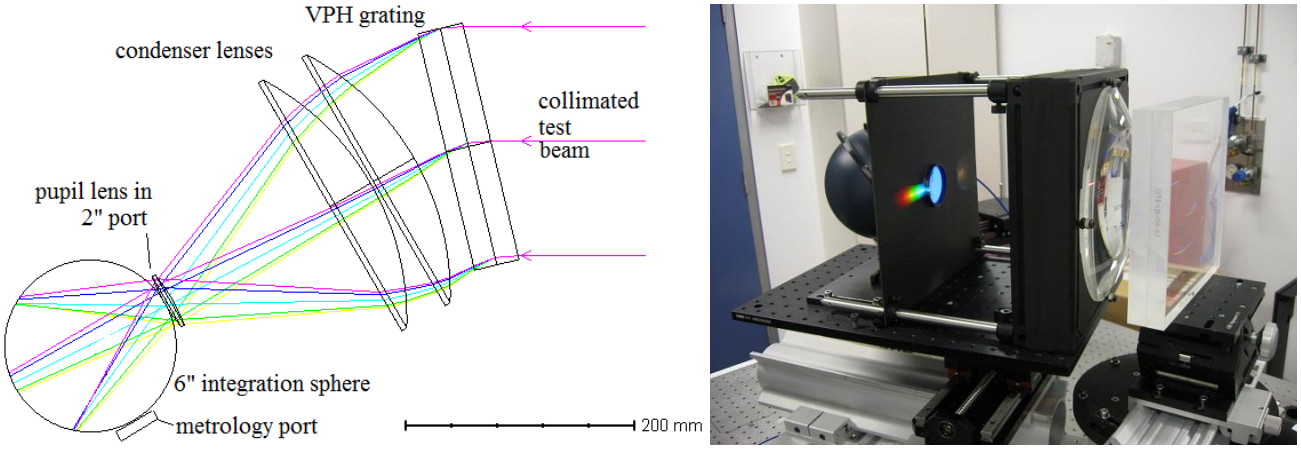


Figure 7. Full aperture photometric setup for Hector beam splitter and VPH grating (left panel). Light collector assembly used to measure diffraction efficiency of a VPH grating (right panel). Note the zeroth and 1st order light dispersed by the grating on the pupil lens baffle.

The pupil lens 50 mm in diameter forms the pupil image on the interior of the integration sphere. Both field and pupil aberrations are high but can be tolerated for this illumination application. Photometric measurements are performed with the help of QEPro Ocean Insight spectrometer fiber fed from the metrology port of the integration sphere.

### 3.2 Optical properties of dicroic beamsplitter

The AAO-MQ contracted Asahi Spectra in Japan to manufacture the dichroic beamsplitter for the Hector spectrograph. The delivered part met and exceeded specifications. The irregularity errors are negligible (Figure 8). Measurements in reflection from the dichroic coating (blue arm) were taken at normal incidence. The transmitted wavefront was obtained at the nominal 24° incidence angle so it represents the actual performance in the red arm of the spectrograph.

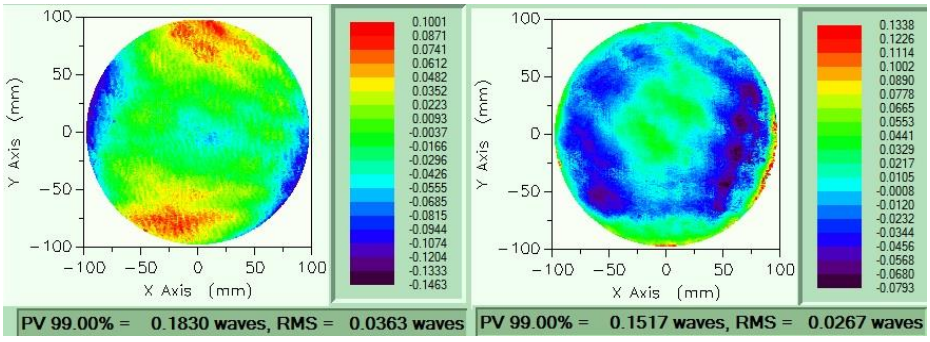


Figure 8. Reflected (left panel) and transmitted wavefront of Hector dichroic beamsplitter (right panel).

Spectral properties of the beamsplitter have been measured at AAO-MQ facilities in great detail (Figure 9). Spectral transmittance and reflectance is determined in collimated light for several incidence angles around the nominal 24° angle. Performance in both arms is excellent with high throughput down to the challenging blue limit. The crossover split area at each angle of incidence has steep slope with a total extent of ~12 nm. At the nominal angle, the crossover split wavelength which corresponds to 50% of maximum, is centered at 581 nm according to specification. At higher angles the spectral response is translated to shorter wavelengths according to the well known coating effect of the blue shift.

Consequently, at lower angles of incidence the same effect results in the opposite translation (Figure 9, left panel). The rate of the blue shift can be evaluated at 1 nm/degree.

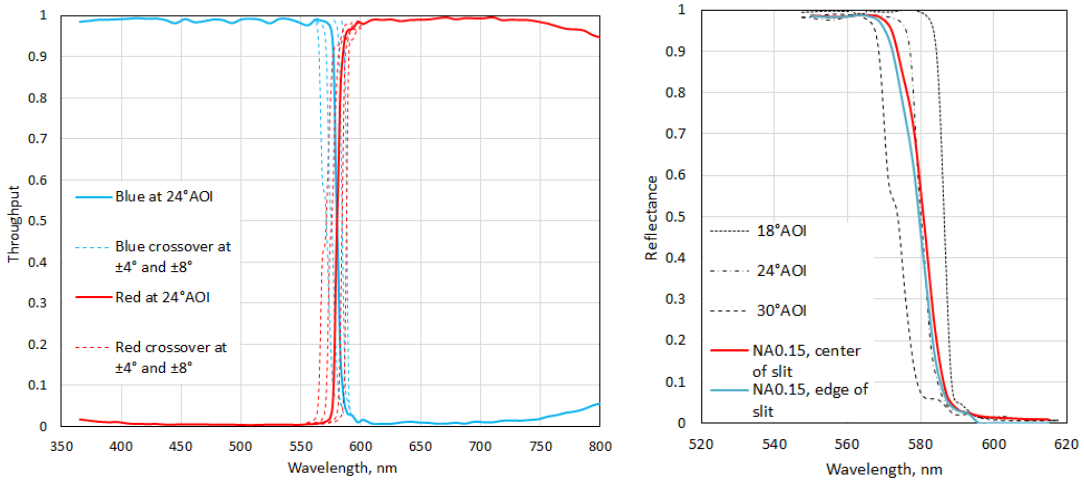


Figure 9. Throughput of dichroic beamsplitter in reflection, blue arm, and in transmission, red arm (left panel). Dichroic crossover region in collimated and divergent beam (right panel).

The dichroic beamsplitter operates in a divergent beam with certain distribution of angles of incidence around the nominal value. This results in reduction of slope of transition and broadening the crossover region (Figure 9). NA0.15 curves were generated by raytracing based on collimated beam measurements. In addition to a shallower and wider transition, modelling reveals dependence of dichroic response on field position in the slit, the peripheral fibers will have a shorter crossover split wavelength by approximately 1.5 nm. As a rule of thumb, an approximate width of dichroic transition can be evaluated as

$$W \approx Wcol + \Delta AOI * Bshift, \quad (2)$$

where

W, Wcol are the width in nm of a dichroic crossover transition in a divergent and collimated beam, respectively;

$\Delta AOI = AOI_{max} - AOI_{min}$ is the range of incidence angles in a divergent beam, degrees;

Bshift is the rate of the blue shift effect, nm/degree

Equation 2 yields a width of ~23 nm for the Hector dichroic. At high incidence angles the value of Wcol is strongly affected by difference in s and p polarizations of a dichroic coating. It is obvious that reduction of the nominal angle of incidence allows to obtain a narrower transition between the arms of the spectrograph. During optical design development, the implementation with the dichroic before the collimator at AOI 24° was favored vs dichroic after the collimator at AOI 45°. This decision proved to be beneficial from a standpoint of dichroic beamsplitter overall performance.

### 3.3 Performance of VPH gratings

Wasatch Photonics was contracted to design and fabricate the VPH gratings for the Hector spectrograph. The vendor also provided AR coatings with the possibility of recoating if correction of flatness were necessary after assembly of AR coated substrates. The gratings were delivered with zonal interferograms over a standard 4 inch apertures with maximum PV value of 1.5 – 1.7 waves. The full aperture interferometry (Figure 10) reveals more details. The gratings will be the limiting elements in the spectrograph imaging performance.

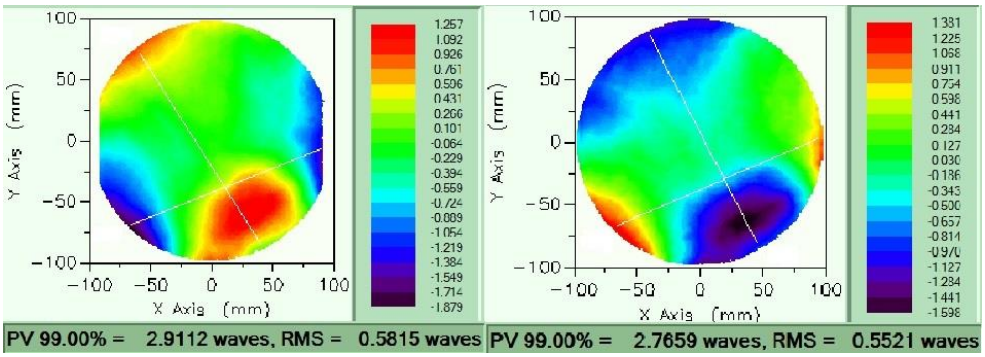


Figure 10. Full aperture transmitted wavefront of Hector gratings in the 1st order: blue VPHG on left panel, red VPHG on right panel.

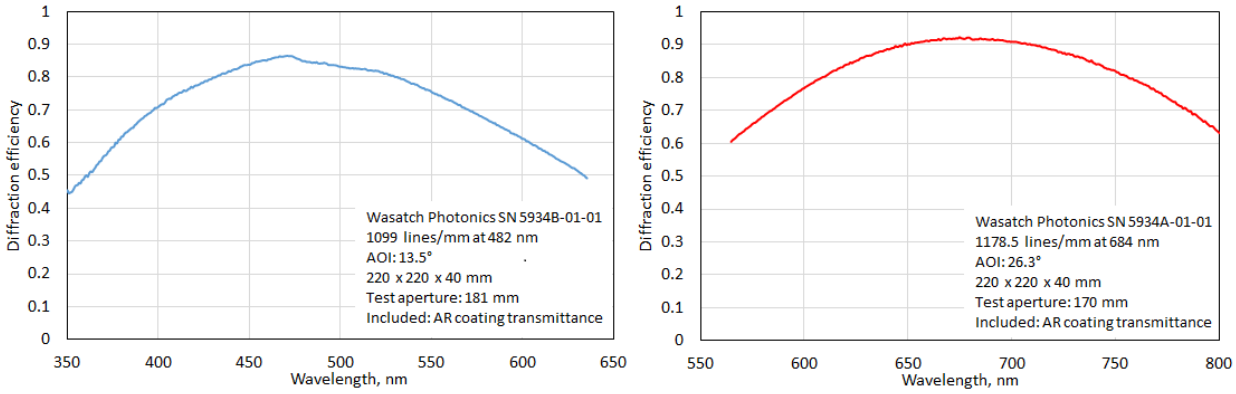


Figure 11. Full aperture diffraction efficiency of Hector gratings: blue VPHG on left panel red VPHG on right panel.

Both gratings have excellent diffraction efficiency in the 1st order (Figure 11). The measurements were made on the laboratory photometric setup (Figure 7). Due to high dispersion, the 2 inch port of the integration sphere could capture only part of the specified wavelength range and three and two separate scans were taken for the blue and red gratings, respectively. The diffraction efficiency curves have been produced by stitching the scans using the areas of overlapping spectra.

### 3.4 Hector spectrograph throughput

Throughput calculations are the mixture of measured and predicted partial contributions for all optical elements. The measured data are used where possible. The dichroic beamsplitter and VPH gratings are measured in house. CCD quantum efficiency was measured by the manufacturer. Transmittance of lenses is determined by internal absorption of materials and reflection losses on AR coated surfaces. Each coating was represented by transmittance at several incidence angles measured on the witness samples from the manufacturer. This metrology was used to predict the spectrograph throughput by means of ray tracing with the model coatings (Figure 12). In so doing, the reflection losses were taken into account as per measured data, whereas, the bulk transmission of lens materials was precisely calculated along the optical path in each element.

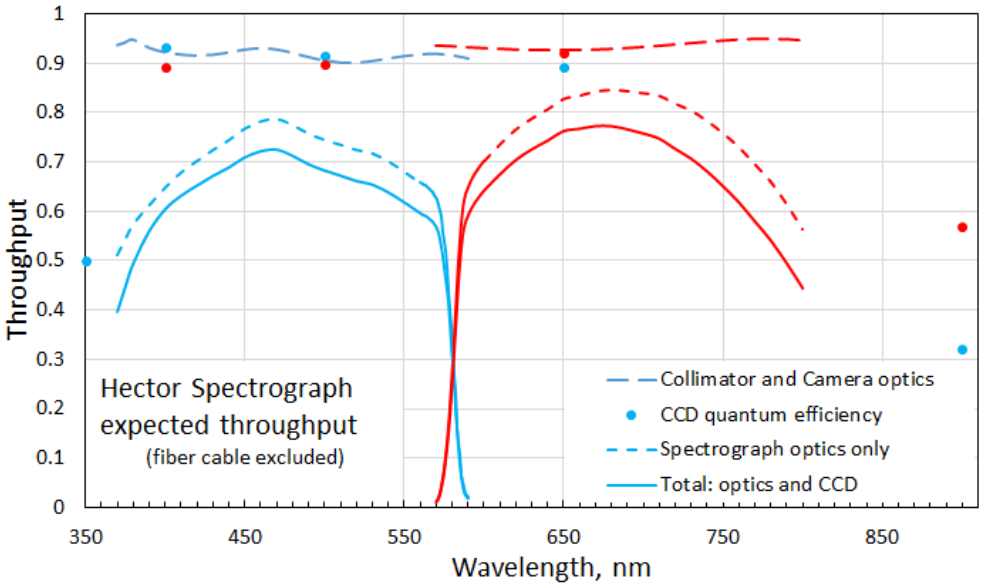


Figure 12. Predicted throughput of Hector blue and red spectrograph arms with contributions of subsystems.

Collimator and camera assemblies are expected to have transmission over 90% due to efficient AR coatings. Somewhat lower values can arise from the modelling limitations of coating reflectance variation from the center to the edge which was replaced by an average value. CCD quantum efficiency is remarkably flat over 400 nm to 650 nm with small differences across the entire range. Neither fiber cable, hexabundles, prisms, sky transmission at the site, telecentricity correction losses nor the losses due to focal ratio degradation are included into the throughput prediction; the assembled spectrograph will be tested with a flat test beam slightly undersized with respect to pseudo-stops and masks. The total throughput of the spectrograph optics including CCD exceeds 70% at maximum.

## 4. SPECTROGRAPH STATUS AND ASSEMBLY PLAN

At present, the spectrograph optics has been delivered and the mechanical structure is assembled and ready for optics integration (Figure 13). The assembly strategy of the spectrograph is based upon by the modular design of its subsystems. The collimators are integrated and interferometrically tested for optical performance on the spectrograph structure. In this all refractive design the cameras are built as subassemblies, they will be tested off the structure in a dedicated interferometric setup. Neither collimators nor cameras are optically corrected on their own, therefore, each one requires a null lens for wavefront quality verification by means of a double pass interferometric test.

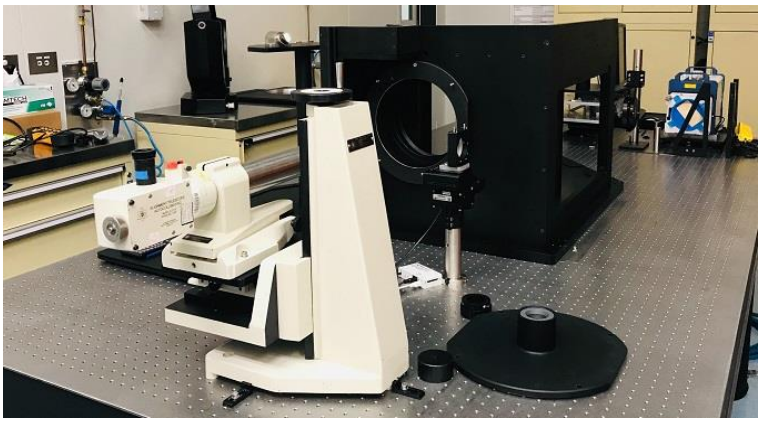

Figure 13. Hector spectrograph structure on optical table in AAO-MQ integration laboratory. Alignment telescope and stage goniometer are set for the spectrograph assembly.

The first step in the alignment process is to establish the optical axis of the system using the slit lens cell and the centered alignment target, and alignment scope. The optical axis, now defined by the alignment scope, is the reference to which all angular and translational degrees of freedom of the remaining optical elements are set. The angles of each component are verified through an additional reference target and a digital stage goniometer. The alignment can start from the last elements, detector windows and flow through the optics to the beamsplitter although this is not particularly critical. Using the kinematic mounting arrangement, any aligned subsystem can be removed and precisely reinstalled. Based on this approach the laboratory alignment will be final, the spectrograph structure will be shipped to the telescope and all the optics remounted kinematically.

Detectors are decentered and tilted with respect to the camera optics. Fine tuning of the detector is best accomplished using the image of a test spectrum from a calibration lamp. The slit is installed into the spectrograph and the optical fiber cable is illuminated with a calibration lamp for the alignment of the spectrograph to be complete. The image quality of the test spectrum and the spectral resolution will be evaluated for compliance with requirements.

## 5. SUMMARY

Hector is a spectroscopic instrument that incorporates a fiber positioning system, an optical spectrograph, and a fiber cable linking the positioner with the spectrograph slit. This paper has described the spectrograph, which is a novel all-refractive 2-arm design delivering a spectral resolution of 0.13 nm over the wavelength range 372-778 nm. All three aspects of the Hector instrument are planned to be installed at the Anglo-Australian Telescope in 2021.

## REFERENCES


[1] Bryant, J., et al., "The SAMI Galaxy Survey: instrument specification and target selection," MNRAS 447, 2857 (2015).

[2] Bryant, J., Bland-Hawthorn, J., Lawrence, J., Croom, S., Brown, D., Venkatesan, S.,Gillingham, P., Zhelem, R., Content, R., Saunders, W., Staszak, N., Van de Sande, J., Couch, W., Leon-Saval, S., Tims, J., McDermid, R., Schaefer, A. "Hector - a new massively multiplexed IFU instrument for the Anglo-Australian Telescope," Proc. SPIE 9908, 99081F (2016).

[3] Bryant, J. J., Bland-Hawthorn, J., Lawrence, J., Saunders, W., Content, R., Croom, S., Venkatesan, S.,Mohanan, M., Brown, R., Wang, A., Zhelem, R., Gillingham, P., Patterson, R., McGregor, H., Couch, W., Van de Sande, J., McDermid, R., Leon-Saval, S., "Hector: a modular integral-field spectrograph instrument for the Anglo-Australian Telescope," Proc. SPIE 10702, 107021H (2018).

[4] Croom, S. M., Lawrence, J. S., Bland-Hawthorn, J., et al., "The Sydney-AAO Multi-object Integral field spectrograph," MNRAS 421, 872 (2012).

[5] Bland-Hawthorn, J., Bryant, J. J., Robertson, G., Gillingham, P., O'Byrne, J., Cecil, G., Haynes, R., Croom, S., Ellis, S., Maack, M., Skovgaard, P., Noordegraaf, D., "Hexabundles: imaging fiber arrays for low-light astronomical applications," Optics Express 19, 2649 (2011).

[6] Content, R., Lawrence, J., Gers, L., Zhelem, R., "Optical design for the TAIPAN and HECTOR transmissive spectrographs," Proc. SPIE 9908, 990888 (2016).

[7] Content, R., Saunders, W., Lawrence, J., Bryant, J., Zhelem, R., "Optical design of the highly cost optimized new Hector Spectrograph," Proc. SPIE 10702, 107028I (2018).